Inorg. Chem. **2007**, *46*, 8238–8244

DFT Study of the Systematic Variations in Metal–Ligand Bond Lengths of Coordination Complexes: the Crucial Role of the Condensed Phase

Rosalie K. Hocking,*,†,§ Robert J. Deeth,*,‡ and Trevor W. Hambley*,†

CHMR, School of Chemistry, The University of Sydney, 2006, Australia, Department of Chemistry, University of Warwick, Coventry, U.K., CV4 7AL

Received June 14, 2007

The experimental M–A and M–B distances in several series of $[MA_nB_{m-n}]$-type complexes have been studied by DFT. Many of the structural features of the series, such as trans influences and sterically induced bond elongations, are not reproduced correctly in gas-phase DFT calculations. However, the correct trends are recovered by explicitly including environmental effects via the COSMO solvation model. These observations imply that the condensed-phase environment plays a critical role in determining the geometric structure of coordination complexes. Thus, any apparently satisfactory reproduction of the condensed-phase structure by an in vacuo calculation may mask an incorrect treatment of the interplay between different ligands attached to the same metal center.

Introduction

Theoretical methods such as density functional theory (DFT) and Hartree−Fock (HF) theory, as well as their extensions, are important tools in coordination chemistry.[1] However, validating computational models for transition metal (TM) systems is problematic. In simple compounds such as diatomic gases and small organic molecules, accurate experimental atomic binding energies and dipole moments can be used to test and calibrate computational methods.[2] Unfortunately, these simple indicators of electronic structure are not available for most TM systems, and therefore, other forms of experimental data must be considered. One of the most bountiful sources of experimental data for TM compounds is structural data and molecular geometries, and these have been widely used to validate computational results for TM complexes.[3−7]

On the whole, DFT appears to provide an excellent basis for computing molecular structure. However, for classical Werner-type coordination complexes, there appears to be a curious anomaly in that the relatively crude local density approximation (LDA) delivers better metal−ligand distances than supposedly more accurate and more sophisticated gradient corrected functionals. Interestingly, the converse applies for organometallic species, prompting the hypothesis that the effect is related to covalency.[3] However, there are three problems with this. First, Solomon et al. have shown that all types of DFT overestimate covalency in such compounds.[8,9] Second, the original calculations were performed in vacuo but compared to condensed-phase experimental data. Third, energy is not particularly sensitive to structure, so the apparently superior performance of the LDA for coordination complexes may not be such a significant result.[1] In fact, in the interests of computational efficiency, some workers deliberately sacrifice structural accuracy by using quite small basis sets for geometry optimizations and then focus on computing good single-point energies using much larger basis sets and/or more sophisticated methods. This approach appears to be quite generally applicable and successful.[10] Thus, if structural data are to be useful for

* To whom correspondence should be addressed. E-mail: rosalie.hocking@csiro.au (R.K.H.); robert.deeth@warwick.ac.uk (R.J.D.); t.hambley@chem.usyd.edu.au (T.W.H.).

† The University of Sydney.

‡ University of Warwick.

§ Current address: CSIRO Land and Water, Urrbrae, Australia.

(1) Bray, M. R.; Deeth, R. J.; Paget, V. J. *Prog. Reaction Kinetics* **1996**, *21*, 169−214.

(2) Scheiner, A. C.; Baker, J.; Andzelm, J. W. *J. Comput. Chem.* **1997**, *18*, 775−795.

(3) Bray, M. R.; Deeth, R. J.; Paget, V. J.; Sheen, P. D. *Int. J. Quantum Chem.* **1996**, *61*, 85−91.

(4) Frenking, G. *J. Organomet. Chem.* **2001**, *635*, 9−23.

(5) Ehlers, A. W.; Frenking, G. *J. Am. Chem. Soc.* **1994**, *116*, 1514−1512.

(6) Dance, I. G.; Harris, H. H.; Wenger, E. *Chem. Eur. J* **2002**, *8*, 3497−3511.

(7) Dance, I. G.; Dean, P. A. W.; Fisher, K. J.; Harris, H. H. *Inorg. Chem.* **2002**, *41*, 3560−3569.

(8) Szilagyi, R. K.; Metz, M.; Solomon, E. I. *J. Phys. Chem. A.* **2002**, *106*, 2994−3007.

(9) Shadle, S. E.; Hedman, B.; Hodgson, K. O.; Solomon, E. I. *Inorg. Chem.* **1994**, *33*, 4235−4255.

(10) Siegbahn, P. E. M.; Blomberg, M. R. A. *Chem. Rev.* **2000**, *100*, 421−437.

10.1021/ic701166p CCC: $37.00
Published on Web 09/01/2007

testing the limits of DFT, we must do more than simply optimize the structures of individual metal complexes and compare them to crystallographic data. One way the energetics of TM bonding can be observed geometrically is through structural changes in series of related compounds. The most well-known of these effects are the structural trans influences.[11,12] Clearly, if there are geometric differences between two related compounds, then a good test of a methodology is to see if the geometry of the two compounds is predicted correctly relative to each other. While trans influences have been reproduced in DFT calculations in specific cases, for example, $[Rh(PR_3)_3Cl]$,[13] no systematic study which addresses series of related compounds has been published. Systematic studies of TM complexes have largely focused on homoleptic compounds due to both the computational time saved in evaluating symmetric species and because spectroscopic observations are simplified by symmetry.[3,8] Therefore, here we set out to evaluate the ability of DFT to reproduce mixed-ligand systems, the geometric effects that ligands have on each other. Three series of compounds $[MA_nB_{m-n}]$ are analyzed, as well as a series where trans influences and steric bulk have an effect on metal−ligand distances. Significant differences between the geometries in the gas phase and the condensed phase are found.

Experimental Methods

DFT Calculations. DFT calculations were performed using the Amsterdam Density Functional (ADF) program suite version 2000.01[14−16] or 2003[17] and the Gaussian 98 program.[18] Starting points for geometry optimizations were taken from crystallographic data where available, and where unavailable, starting structures were created from existing crystallographic fragments.[19,20]

Calculations Performed Using ADF. Geometries optimized using the local density approximation (LDA)[21] used the Vosko−Wilk−Nusair correlation functional (VWN).[22] Gradient-corrected calculations were performed using the exchange functional of Becke[23] and the correlation functional of Perdew[23,24] (BP86). The lowest energy geometries of the series $[PtCl_n(NH_3)_{4-n}]^{2-n}$, $[PtCl_n(CO)_{4-n}]^{2-n}$ ($n = 0-4$), and subsets of the series $[NiN_n(H_2O)_{6-n}]^{2-n}$, $[NiN_n(O-R)_{6-n}]^{4-n}$ ($n = 0-6$), where O−R is an anionic oxygen donor, were considered. Gas-phase calculations used the convergence criteria of integration level 6, as defined by ADF[25] and condensed phase used COSMO integration level 3.[26]

The frozen core approximation[27] was used for the 1s−4d orbitals for platinum, 1s−2p orbitals for cobalt, nickel, and chlorine, and the 1s orbital of nitrogen, oxygen, and carbon. Scalar relativistic corrections[28,29] to the LDA were applied for all calculations on the Pt^{II} species. For valence orbitals, Slater-type orbital (STO) basis sets of triple-ζ quality were employed with polarization functions on the ligand atoms (2p for H, 3d for the rest) and additional valence p orbitals on the metal atoms, i.e., ADF basis set IV.[30,31] This basis set combination was chosen, as previous studies have shown that it gives a well-converged solution.[10,32]

Where implicit solvation was applied, this was done using the COnductor-like Screening MOdel (COSMO).[33−35] Nonbonded radii used (in Å) were Cl = 1.725, N = 1.608, H = 1.350, C = 1.700, O = 1.517, Pt = 1.992, and Ni = 1.750. A dielectric constant of 78.8 (water) and an outer cavity radius of 1.9 Å were further used to parametrize the COSMO solvation cavity.[14−16] Population analysis was performed using Mulliken[36] populations as implemented by ADF. To compare relative orbital energies between the solvated and gas phase for the $[PtCl_n(NH_3)_{4-n}]^{2-n}$ series, the lowest lying Pt orbital was set to −102 eV for all compounds.

Calculations Performed Using Gaussian98. Calculations involving cobalt were performed with the basis set 6-311G* on the metals and 6-31G* on the ligands, again as this level of theory/basis set combination has been shown by others to give a theoretically well-converged solution.[10,32,37−39] Solvation corrections were added with the polarized continuum model and a dielectric of 78.4, as implemented by Tomasi and co-workers.[40−43] The value

(11) Appleton, T. G.; Clark, H. C.; Manzer, L. E. *Coord. Chem. Rev.* **1973**, *10*, 335−422.
(12) Coe, B. J.; Glenwright, S. J. *Coord. Chem. Revs.* **2000**, *203*, 5−80.
(13) Deeth, R. J. *J. Chem. Soc. Dalton Trans.* **1993**, 3711−3713.
(14) Versluis, L.; Ziegler, T. *J. Chem. Phys.* **1988**, *88*, 322−328.
(15) Baerends, E. J.; Ellis, D. E.; Ros, P. *Chem. Phys.* **1973**, *2*, 41−51.
(16) Baerends, E. J.; Berces, A.; Bo, C.; Boerrigter, P. M.; Cavallo, L.; Deng, L.; Dickson, R. M.; Ellis, D. E.; Fan, L.; Fischer, T. H.; Fonseca Guerra, C.; van Gisbergen, S. J. A.; Groaeneveld, J. A.; Gritsenko, O. V.; Harris, F. E.; van den Hoek, P.; Jacobsen, H.; van Kessel, G.; Kootstra, F.; van Lengthe, E.; Osinga, V. P.; Philipsen, P. H. T.; Post, D.; Pye, C. C.; Ravenek, W.; Ros, P.; Schipper, R. T.; Schreckenbach, G.; Snijders, J. G.; Sola, M.; Swerhone, D.; teVelde, G.; Vernooijs, P.; Versluis, L.; Visser, O.; van Wezenbeek, E.; Wiesenekker, G.; Wolff, S. K.; Woo, T. K.; Ziegler, T. *ADF Program System*; Scientific Computing and Modeling: Amsterdam, 2000.
(17) Note that good agreement was found between ADF2001 and ADF2003.
(18) Frisch, M. J.; Trucks, G. W.; Schlegel, H. B.; Scuseria, G. E.; Robb, M. A.; Cheeseman, J. R.; Zakrzewski, V. G.; Montgomery, J. A., Jr.; Stratmann, R. E.; Burant, J. C.; Dapprich, S.; Millam, J. M.; Daniels, A. D.; Kudin, K. N.; Strain, M. C.; Farkas, O.; Tomasi, J.; Barone, V.; Cossi, M.; Cammi, R.; Mennucci, B.; Pomelli, C.; Adamo, C.; Clifford, S.; Ochterski, J.; Petersson, G. A.; Ayala, P. Y.; Cui, Q.; Morokuma, K.; Malick, D. K.; Rabuck, A. D.; Raghavachari, K.; Foresman, J. B.; Cioslowski, J.; Ortiz, J. V.; Stefanov, B. B.; Liu, G.; Liashenko, A.; Piskorz, P.; Komaromi, I.; Gomperts, R.; Martin, R. L.; Fox, D. J.; Keith, T.; Al-Laham, M. A.; Peng, C. Y.; Nanayakkara, A.; Gonzalez, C.; Challacombe, M.; Gill, P. M. W.; Johnson, B. G.; Chen, W.; Wong, M. W.; Andres, J. L.; Head-Gordon, M.; Replogle, E. S.; Pople, J. A. *Gaussian 98*, revision A.7; Gaussian, Inc.: Pittsburgh, PA, 1998.
(19) Allen, F. H.; Davies, J. E.; Galloy, J. J.; Johnson, O.; Kennard, O.; Macrae, C. F.; Mitchell, E. M.; Mitchell, G. F.; Smith, J. M.; Watson, D. G. *J. Chem. Inf. Comput. Sci.* **1991**, *31*, 187−204.
(20) Allen, F. H.; Kennard, O. *Chem. Des. Autom. News.* **1993**, *8*, 31−37.
(21) Slater, J. C. *Adv. Quant. Chem.* **1972**, *6*, 1.
(22) Vosko, S. H.; Wilk, L.; Nusair, M. *Can. J. Phys.* **1980**, *58*, 1200−1211.
(23) Becke, A. D. *Phys. Rev. A* **1988**, *38*, 3098−3100.
(24) Perdew, J. P. *Phys. Rev. B* **1986**, *33*, 8822−8824.
(25) *Scientific Computing and Modelling NV., ADF User's Guide*; SCM: Amsterdam, 1999.
(26) Condensed-phase calculations cannot converge to the same degree of accuracy as gas-phase calculations because of the tessellated potential energy surface.
(27) Baerends, E. J.; Ellis, D. E.; Ros, P. *Theor. Chim. Acta* **1972**, *27*, 339−354.
(28) Snijders, J. G.; Baerends, E. J.; Ros, P. *Mol. Phys.* **1979**, *38*, 1909−1929.
(29) Snijders, J. G.; Baerends, E. J. *J. Mol. Phys.* **1978**, *36*, 1789.
(30) Vernooijs, P.; Snijders, G. P.; Baerends, E. J. *Slater Type Basis Functions for the Whole Periodic System*, Internal Report; Free University: Amsterdam, 1981.
(31) Snijders, J. G.; Vernooijs, P.; Baerends, E. J. *At. Data. Nucl. Data Tab.* **1981**, *26*, 483−485.
(32) Ryde, U.; Olsson, M. H. M.; Pierloot, K. The Structure and Function of Blue Copper Proteins. In *Theoretical and Computational Chemistry*; Elsevier: Amsterdam, London, 2001; Vol. 9, pp 1−55.
(33) Klamt, A. *J. Chem. Phys.* **1995**, *99*, 2224−2235.
(34) Klamt, A.; Jones V. *J. Chem. Phys.* **1996**, *105*, 9972−9981.
(35) Klamt, A.; Schuurmann, G. *J. Chem. Soc: Perkin Trans 2* **1993**, 799−805.
(36) Mulliken, R. S. *J. Chem. Phys.* **1955**, *23*, 1833−1840.
(37) Rassolov, V. A.; Pople, J. A.; Ratner, M. A.; Windus, T. L. *J. Chem. Phys.* **1998**, *109*, 1223−1229.
(38) McGrath, M. P.; Radom, L. *J. Chem. Phys.* **1995**, *103*, 6104−6113.
(39) Curtiss, L. A.; McGrath, M. P.; Blaudeau, J. P.; Davis, N. E.; Binning, R. C. J.; Radom, L. *J. Chem. Phys.* **1995**, *103*, 6104−6113.

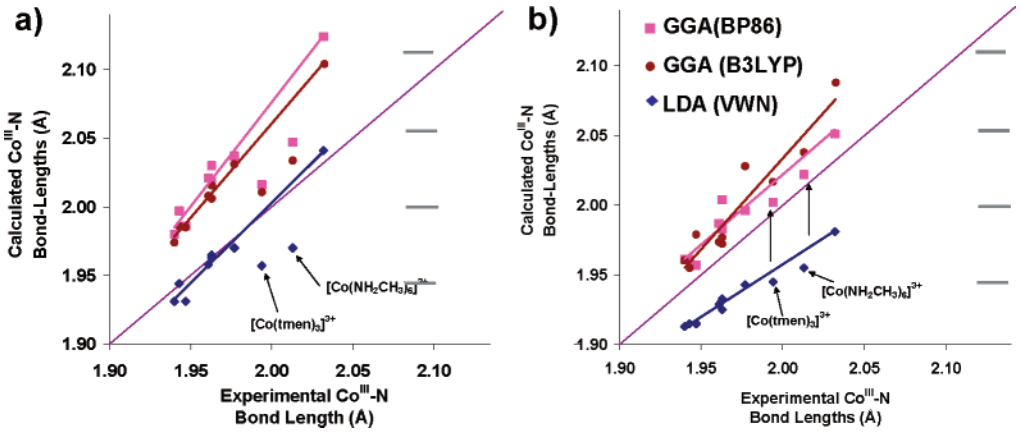

Figure 1. Plots of experimental vs calculated bond distances for a series of Co(III) hexaamine compounds. The purple line represents a 1:1 relationship between the calculation and the experiment. Data above the line indicate an overestimation of metal−ligand bond lengths, below the line an underestimation. Graph (a) shows gas-phase calculation, graph (b) condensed-phase (solvated) calculations.

of 78.4 (water ϵ) was chosen because it has been used previously. The effects described herein were found to depend only slightly on the value of ϵ that is chosen (see Figure S6 for a comparison of $\epsilon = 1.4$ and 100).

Extraction of Crystallographic Data. The results of the DFT calculations were compared to crystallographic data available from the CSD. The program CONQUEST[44,45] was used to extract structural properties. Where more than one suitable structure existed, equivalent bond lengths were averaged, and the error quoted is the confidence interval on the mean, as detailed elswhere.[46,47] In all cases, only structures with R values <7.5% were used for comparison.

Results and Discussion

Analysis of Metal−Ligand Bond Lengths. Throughout this work, metal−ligand interactions have been analyzed using groups of crystal structures. Analysis of groups of structures is important as it enables us to "average" the effects of crystal packing. In this way we can compare the effects of "average environment" with the results of DFT calculations in the gas and condensed phase.[46,48−50]

1. Reduction of Bond Length upon the Inclusion of Solvation Corrections. Figure 1 shows the plots of experimental vs calculated Co^{III}−N bond lengths for the series of Co^{III} hexaamine compounds illustrated in Figure S1.[51−57] The structures were calculated at three different levels of theory: applying the LDA (blue diamonds), the gradient-corrected functional BP86 (pink squares), and the hybrid functional B3LYP (red circles). In each plot, a purple line representing a 1:1 relationship between calculated structures and experimental structures is shown. Thus, points above the line represent an overestimation of metal−ligand bond lengths, and points below the line an underestimation.

It is clear from Figure 1a that the bond lengths are systematically overestimated using the BP86 and B3LYP functionals, while results closer to the experiment are generated using the LDA. This observation is consistent with the work of other authors who have noted that, of the DFT methods, LDA best reproduces the geometries of Werner-type compounds.[3] From the graphs, it is also clear that the two complexes $[Co(tmen)_3]^{3+}$ and $[Co(NH_2CH_3)_6]^{3+}$ behave as outliers.

The application of the solvation model (Figure 1b) reduces the bond lengths in each series, though a small systematic overestimation of bond lengths remains. The reduction in bond lengths across the series of Co^{III} hexaamines by the application of the solvation model is not uniform. In particular, inclusion of solvation has the least effect on the two species with the largest amount of steric bulk, $[Co(tmen)_2]^{3+}$ and $[Co(NH_2CH_3)_6]^{3+}$, bringing them back into line with the rest of the series.[26,58] This is presumably because the effect of solvation depends on how protected a metal−ligand bond is from the environment. In systems with a large amount of steric bulk, the ligand-based orbitals are less exposed to the effects of the environment, shown schematically in Figure S2. Consequently, solvation corrections have a greater effect on compounds with less-bulky ligands. This

(40) Mennucci, B.; Cances, E.; Tomasi, J. *J. Phys. Chem. B* **1997**, *101*, 10506−10507.
(41) Mennucci, B.; Tomasi, J. *J. Chem. Phys.* **1997**, *106*, 5151−5152.
(42) Cammi, R.; Mennucci, B.; Tomasi, J. *J. Phys. Chem. A* **1999**, *103*, 9100−9102.
(43) Cammi, R.; Mennucci, B.; Tomasi, J. *J. Phys. Chem. A* **2000**, *104*, 5631−5632.
(44) *Quest 3D, a program for searching the CSD*; CCDC: Cambridge, UK, 1994.
(45) *Vista, a program for the analysis and display of data retrieved from the CSD*; CCDC: Cambridge, UK, 1996.
(46) Hocking, R. K.; Hambley, T. W. *Inorg. Chem.* **2002**, *21*, 2660−2666.
(47) Orpen, A. G.; Quayle, M. J. *J. Chem. Soc. Dalton Trans.* **2001**, 1601−1610.
(48) Hocking, R. K.; Hambley, T. W. *Inorg. Chem.* **2003**, *42*, 2833−2835.
(49) Hocking, R. K.; Hambley, T. W. *Dalton Trans.* **2005**, 969−978.
(50) Hocking, R. K.; Hambley, T. W. *Organometallics* **2007**, *26*, 2815−2823.
(51) Brunner, H.; Ludi, A.; Raselli, A.; Bürgi, H.-B. *Helv. Chim. Acta* **1996**, *79*, 1607−1610.
(52) Yoneda, H. Unpublished data.
(53) Henrick, K.; McPartlin, M.; Munjoma, S.; Owston, P. G.; Peters, R.; Sangokoya, S. A.; Tasker, P. A. *J. Chem. Soc. Dalton Trans.* **1982**, 225−227.
(54) Bernhardt, P. V.; Lawrence, G. A.; Hambley, T. W. *J. Chem. Soc., Dalton Trans.* **1989**, 1059−1065.
(55) Bernhardt, P. V.; Jones, L. A. *J. Chem. Soc., Dalton Trans* **1998**, 1757−1761.
(56) Hambley T. W.; Searle G. H.; Snow M. R. *Aust. J. Chem.* **1982**, *35*, 1285−1295.
(57) Ishi, M.; Umehara, M.; Harada, K.; Nakahara, M. *Bull. Chem. Soc. Jpn.* **1987**, *60*, 2683−2685.
(58) Comba, P.; Hambley, T. W. *Molecular Modelling of Inorganic Compounds*, 2nd ed.; Wiley-VCH: Weinheim, 2001.

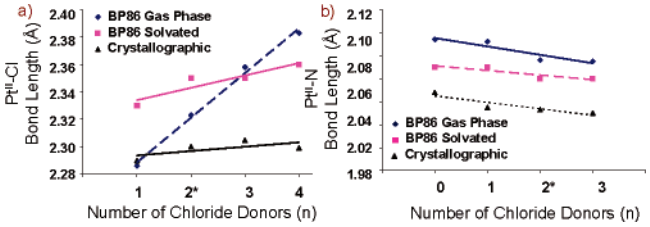

Figure 2. (a) $Pt^{II}-Cl$ and (b) $Pt^{II}-N$ bond lengths for the series of compounds $[PtCl_n(NH_3)_{4-n}]^{2-n}$ ($n = 0-4$). Structures are calculated in the gas phase (blue diamonds) and with the addition of solvation corrections (pink squares), and crystallographic data are given by the black triangles. The asterisks indicate that the bond lengths of cis and trans isomers were averaged. The dagger indicates that all Pt−Cl bond lengths were averaged.

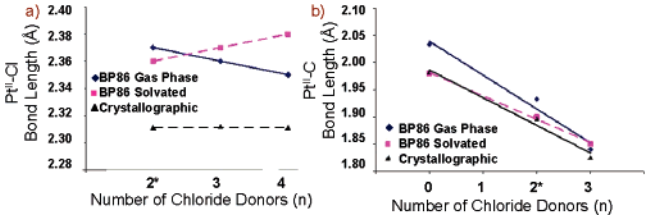

Figure 3. Effect of solvation on the calculation of (a) $Pt^{II}-Cl$ and (b) $Pt^{II}-C$ bond lengths in $[PtCl_n(CO)_{4-n}]$. Structures are calculated in the gas phase (pink squares) and with the addition of solvation corrections (blue diamonds), and crystallographic data are given by the black triangles. The asterisk indicates that only crystallographic data for the cis isomer of $[PtCl_2(CO)_2]$ have been reported. The dagger indicates that all Pt−Cl bond lengths were averaged.

observation also suggests that the dielectric of the crystal environment is sufficient to quantifiably change the bonding properties of ligands.

We also note that the performance of the LDA in reproducing M−L bond lengths[3] results from the LDA overbinding compensating for the effect of the environment. Gas-phase gradient-corrected functionals give longer M−L distances than the LDA, but upon addition of solvation corrections, both sets of bond lengths get shorter, making the LDA distances shorter than the experimental and the gradient-corrected distances relatively close to those observed experimentally (Figure 1).

2. Mutual Ligand Effects. It was shown above that the environment has a pronounced effect on metal−ligand bond lengths and that this effect depends on how sterically protected that bond is from the environment. Thus, we considered it important to assess the effect that the environment had on mutual ligand effects. To do this, we have chosen to study a series of compounds where the electronic interdependencies of the ligands have measurable structural effects.

2.1. $[PtCl_n(NH_3)_{4-n}]^{2-n}$ and $[PtCl_n(CO)_{4-n}]^{2-n}$, $n = 0-4$. To understand the structural effects of systematically varying ligands, two series were chosen for study: $[PtCl_n(NH_3)_{4-n}]^{2-n}$ and $[PtCl_n(CO)_{4-n}]^{2-n}$, where $n = 0-4$. The series were chosen, as they are well characterized structurally[59,60] and exhibit quite different ligand interdependencies. In the $[PtCl_n(NH_3)_{4-n}]^{2-n}$ series, no structurally obvious mutual ligand effects are present, i.e., the $Pt^{II}-Cl$ and $Pt^{II}-N$ bond lengths remain constant (within crystallographic resolution) throughout the series (Figure 2, Table S5). In contrast, in the series $[PtCl_n(CO)_{4-n}]$ an interdependence between the donor atoms is observed: the $Pt^{II}-C$ bond lengths range from 1.825 Å in $[PtCl_3CO]^-$ to 1.982 Å in $[Pt(CO)_4]^{2+}$. The differences in bond lengths arising because of differences in π back-donation, which have been characterized elsewhere.[61] No statistically significant variation in $Pt^{II}-Cl$ bond lengths is observed throughout either series experimentally.

From a computational perspective, both series involve anionic (Cl^-) and neutral (NH_3 or CO) ligands and have high symmetry. The square planar geometry and d^8 electron configuration of Pt(II) also means that all four ligands interact σ-wise with the empty Pt $5d_{x^2-y^2}$ orbital, simplifying MO analysis.[25]

Figures 2 and 3 show the results of experiment (black triangles), gas-phase calculations (blue diamonds), and condensed phase calculations (pink squares) for the $[PtCl_n(NH_3)_{4-n}]^{2-n}$ series (Figure 2) and the $[PtCl_n(CO)_{4-n}]^{2-n}$ series (Figure 3). Two observations emerge from geometry optimizations in the gas phase. First, the $Pt^{II}-Cl$ bond lengths calculated in the gas phase show a difference from those determined experimentally in that the systematic increase with the number of Cl donors in the coordination sphere is overestimated. In contrast to the bonds to the Cl ligands, the bonds to the NH_3 and CO ligands are uniformly overestimated and show similar trends to the $Co^{III}-N$ bonds described above.[46]

The solvation models (COSMO in ADF and PCM in Gaussian98 calculations, respectively) were applied to each series to examine whether the effect of anionic donors could be modified. It was found that the application of the solvation models dampened the large variation in $Pt^{II}-Cl$ bond lengths, approximately reproducing the experimental trend across the $[PtCl_n(NH_3)_{4-n}]^{2-n}$ series (Figure 3). In addition, when solvation corrections are added, a reduction in $Pt^{II}-N$ bond lengths is seen, similar to the reduction in bond lengths observed for the $[Co^{III}N_6]$ series (Figure 1). Even though the bond lengths trends are reproduced correctly, the calculated bond lengths are still slightly overestimated, consistent with the observations noted above for the Co^{III} hexaamines.[3]

The addition of a solvation model to the series $[PtCl_n(CO)_{4-n}]^{2-n}$ had different effects to those seen for the $[PtCl_n(NH_3)_{4-n}]^{2-n}$ series. The inconsistencies noted in $Pt^{II}-Cl$ bond lengths when compared to the experiment were not altered substantially by the addition of a solvation model (Figure 4), and Pt−C distances were generally well produced by both gas-phase and condensed-phase calculations, though there is a small improvement on including solvation. The difference may be reflective of the fact that Pt−CO bonds are much more covalent than $Pt-NH_3$ bonds.

(59) Bagnoli, F.; Dell' Amico, D. B.; Calderazzo, F.; Englert, U.; Marchetti, F.; Herberich, G. E.; Pasqualetti, N.; Ramello, S. *J. Chem. Soc. Dalton Trans.* **1996**, 4317−4318.
(60) Willner, H.; Bodenbinder, M.; Broechler, R.; Hwang, G.; Rettig, S. J.; Trotter, J.; von Ahsen, B.; Westphal, U.; Jonas, V.; Thiel, W.; Aubke, F. *J. Am. Chem. Soc.* **2001**, 123, 588−602.
(61) Hocking, R. K.; Hambley, T. W. *Chem. Comm.* **2003**, *13*, 1516−1517.

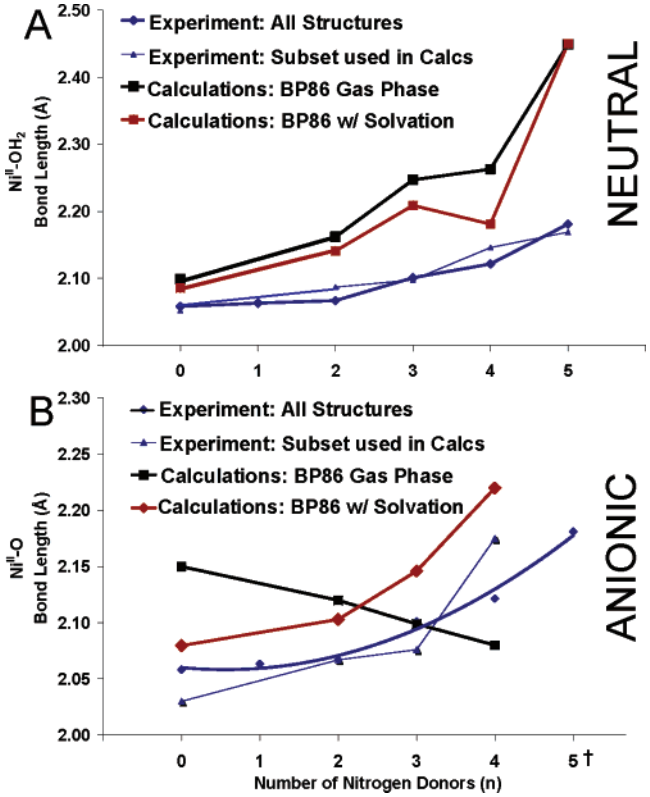

Figure 4. Comparison of calculations and experimental Ni−O distances for two series (A) $[Ni(NR_3)_n(H_2O)_{6-n}]^{2+}$ and (B) $[Ni(NR_3)_n(O-R)_{6-n}]^{n-4}$, where NR_3 represents an sp^3-hybridized N donor. The thick blue curves represent the experimental average $Ni^{II}-O$ distances reported in ref 46. The thinner blue curves represent the series of structures used as a subset for the DFT calculations.

2.2. $[Ni(O-R)_{6-n}(NR_3)_n]^{n-4}$ and $[Ni(H_2O)_{6-n}(NR_3)_n]^{2+}$, $n = 0-6$, $NR_3 = sp^3$-Hybridized N Donor. Two other series MA_nB_m were studied. Series A comprised of $[Ni(H_2O)_{6-n}(NR_3)_n]^{2+}$ and series B $[Ni(O-R)_{6-n}(NR_3)_n]^{n-4}$ where O = anionic donor oxygen donor. These series of compounds provide a useful comparison here, as it has been shown that that both the Ni−N and Ni−O bond distances increase as the number of N donors in the coordination sphere increases.[46] Further, it can be shown by analysis of subsets of crystallographic data that the trend is independent of the charge on the oxygen donor (blue line, Figure 4A and B and Figure S3).[46] Gas-phase DFT calculations (shown by black squares) generate the correct trends for series A, (Figure 4A) and incorrect trends for Series B (Figure 4B). Upon the addition of solvation corrections, the geometric trends in both series are qualitatively correct, shown by the red squares, though, as before, the metal−ligand bond lengths are overestimated. This overestimation is particularly notable in the structure of $[Ni(NH_3)_5(H_2O)]^{2+}$. It has been noted elsewhere[62−64] that the water molecule is extremely labile in this complex and this overestimation of the bond length may be related to the lability.

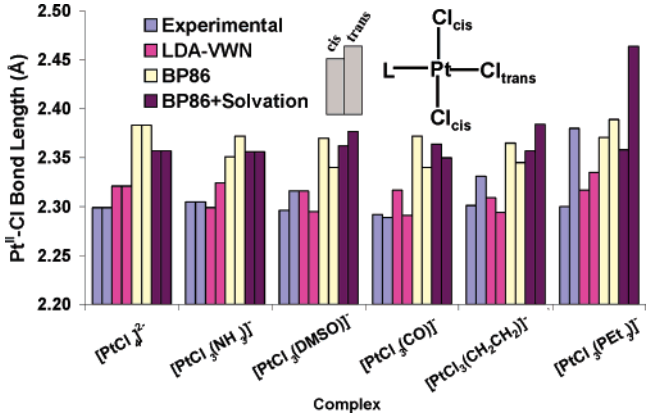

Figure 5. Comparison of the calculated and experimental bond lengths of a series of platinum(II) compounds of the form $[Pt^{II}Cl_3X]$, where X = Cl, NH_3, DMSO, CO, CH_2CH_2, and PEt_3, whose $Pt^{II}-Cl$ bonds are subject to different structural trans influences.

2.3. Trans Influences. A body of work that dealt with the electronic interdependence of ligands would be incomplete if it did not examine structural trans influences.[11] In Figure 6, the experimental and calculated bond lengths are plotted for the series of compounds, $[PtCl_4]^{2-}$, $[PtCl_3(NH_3)]^-$, $[PtCl_3(DMSO)]^-$, $[PtCl_3(CO)]^-$, $[PtCl_3(CH_2CH_2)]^-$, and $[PtCl_3(PEt_3)]^-$. For the complexes $[PtCl_3(NH_3)]^-$, $[PtCl_3(DMSO)]^-$, and $[PtCl_3(CH_2CH_2)]^-$, the gas-phase calculations do not produce cis/trans trends in the $Pt^{II}-Cl$ bond lengths consistent with the experimental observations. Upon the addition of solvation corrections, the correct cis/trans trends in $Pt^{II}-Cl$ bond lengths are obtained for all six complexes tested.

In addition to the Pt complexes, a number of cobalt pentaammine species, (e.g., $[Co(NH_3)_5L]^{x+}$) subject to different structural trans effects have been studied, Table S8. They show trends analogous to those seen for the Pt complexes.

3. Analysis of Molecular Orbitals. To characterize the observations of mixed-ligand systems further, both the coefficients of mixing (Table 1) and the orbital energies (Figure 6) of the $[PtCl_n(NH_3)_{4-n}]^{2-n}$ series were considered.

Table 1 gives the composition of the unoccupied Pt $5d_{x^2-y^2}$ orbital for the $[PtCl_n(NH_3)_{4-n}]^{2-n}$ series. There is little difference in the metal−ligand mixing between solvated and gas-phase calculations for $[PtCl_4]^{2-}$ and $[Pt(NH_3)_4]^{2+}$. However, when the mixed-ligand systems are compared, the Cl(p) contribution decreases and the N(p) contribution increases upon the addition of solvation corrections.

Figure 6 shows the relative orbital energies of the five compounds $[PtCl_4]^{2-}$ (blue), *cis*-$[PtCl_2(NH_3)_2]$ (red), *trans*-$[PtCl_2(NH_3)_2]$, $[PtCl(NH_3)_3]^+$ (gray), and $[Pt(NH_3)_4]^{2+}$ (purple). In each case, the orbitals have been adjusted to the same scale by calibration to a low-lying Pt(s) orbital. For each compound, two sets of MOs are given: to the left (dark) the gas-phase calculations and to the right (light) those from the condensed phase. The Cl(p) orbitals are marked with a gray bar, and the N(p) orbitals are marked with a black bar, black arrows indicate the relative changes upon going from gas-phase to condensed-phase calculations. There is little

(62) Margerum, D. W.; Cayley, G. R.; Weatherburn, D. C.; Pagenkopf G. K. Kinetics and Mechanism of Complex Formation and Ligand Exchange. In *Coordination Chemistry*; Martell, A. E., Ed.; American Chemical Society: Washington, DC, 1978; pp 1−220.
(63) Jones, J. P.; Billo, E. J.; Margerum, D. W. *J. Am. Chem. Soc.* **1970**, *92*, 1875−1880.
(64) Margerum, D. W.; Rosen, H. M. *J. Am. Chem. Soc.* **1967**, *89*, 1088−1092.

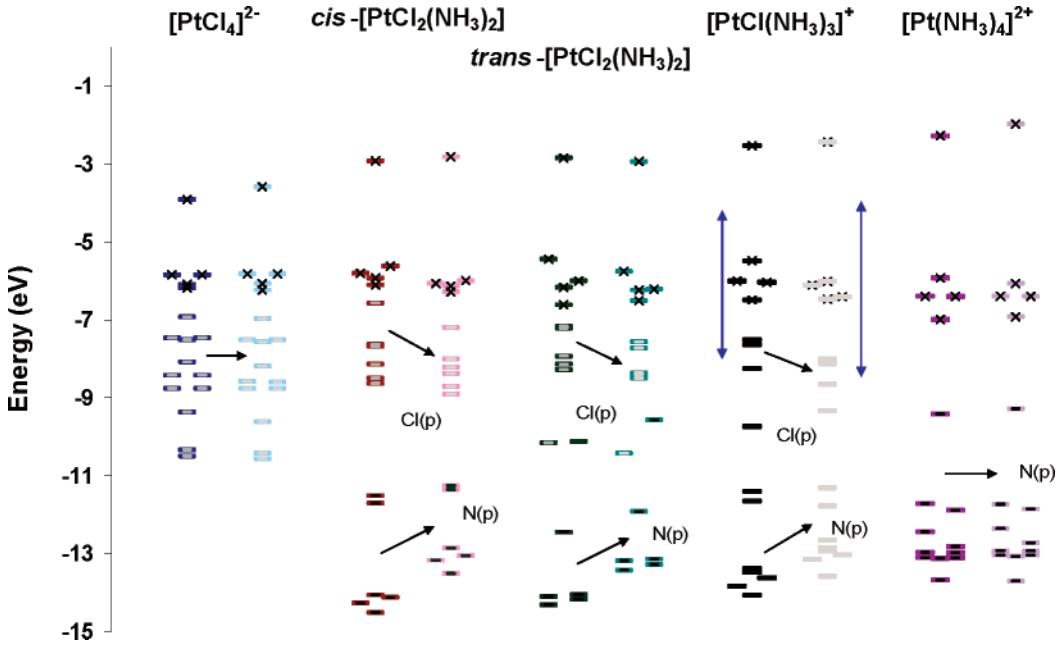

Figure 6. Gas-phase (left, dark) and condensed-phase (right, light) orbital energies of $[PtCl_4]^{2-}$, *cis*-$[PtCl_2(NH_3)_2]$, *trans*-$[PtCl_2(NH_3)_2]$, $[PtCl(NH_3)_3]$, and $[Pt(NH_3)_4]^{2+}$. Energy levels that are mostly Pt(d) are marked with ×, levels that are mostly Cl(p) have a gray bar, and orbitals which are mostly N(p) have a black bar. Black arrows indicate the changes in gas-phase relative to condensed-phase calculations; vertical blue arrows indicate the energy difference between the Pt(d) and Cl(p) manifolds.

Table 1. Composition of the LUMO (the Pt $5d_{x^2-y^2}$ Based Orbital) in the Gas Phase and Condensed Phase for the Series $[PtCl_n(NH_3)_{4-n}]^{2-n}$

compound	coefficients of mixing for the LUMO
$[PtCl_4]^{2-}$	48%Pt(d) + 52%Cl(p), gas phase
	50%Pt(d) + 50%Cl(p), condensed phase
$[PtCl_3(NH_3)]^-$	47%Pt(d) + 42%Cl(p) + 11% N(p), gas phase
	50%Pt(d) + 41%Cl(p) + 10% N(p), condensed phase
cis-$[PtCl_2(NH_3)_2]$	46%Pt(d) + 29%Cl(p) + 17% N(p), gas phase
	50%Pt(d) + 24%Cl(p) + 22% N(p), condensed phase
trans-$[PtCl_2(NH_3)_2]$	50%Pt(d) + 33%Cl(p) + 17% N(p), gas phase
	52%Pt(d) + 34%Cl(p) +14% N(p), condensed phase
$[PtCl(NH_3)_3]^+$	50%Pt(d) + 18%Cl(p) + 25% N(p), gas phase
	50%Pt(d) + 14%Cl(p) + 29% N(p), condensed phase
$[Pt(NH_3)_4]^{2+}$	56%Pt(d) + 44%N(p), gas phase
	57%Pt(d) + 43%N(p), condensed phase

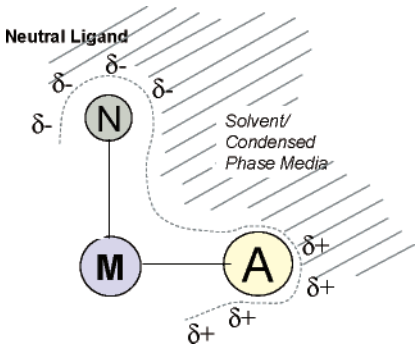

Figure 7. Illustration of how the continuum models effects anionic and neutral donors differently.

change in the relative energy of the Pt(d) orbitals and the ligand (p) manifolds in the two homoleptic compounds $[PtCl_4]^{2-}$ and $[Pt(NH_3)_4]^{2+}$. However, for *cis*-$[PtCl_2(NH_3)_2]$, *trans*-$[PtCl_2(NH_3)_2]$, and $[PtCl(NH_3)_3]^+$, the condensed phase changes the relative energies of the Cl(p) and N(p) manifolds. The Cl(p) orbitals decrease, and the N(p) orbitals increase in energy relative to the Pt(d) orbitals upon solvation, as indicated by the black arrows in Figure 6.

There are two contributions to the relative energy of a ligand manifold and a metal manifold in a complex: first, their relative energies before bonding and, second, any change in energy due to bonding. This makes determining the origin of an orbital energy difficult. PCM and COSMO solvation models act by making the net flux through a surface a given distance away from the outer surface of the molecule zero. This means for an anionic ligand that a δ^+ charge is present at a given distance away. Thus, the opposite side of the molecule has δ^-. The effect on the platinum complexes here is illustrated schematically in Figure 7. The trends in orbital manifolds observed in Figure 6 are consistent with this change; in mixed-ligand complexes, the anionic Cl donors sink in energy and the neutral N donors rise upon the addition of solvation corrections. This observation tells us that ligand manifolds derive an influence from one another that changes upon the addition of solvation such that in mixed-ligand complexes the Cl(p) manifold is closer to the Pt(d) manifold in the gas phase relative to the condensed phase, whereas for N(p) it is the reverse.

This observation gives us insight into the origin of the geometric differences between the condensed-phase and gas-phase calculations. If two molecular orbitals are closer in energy, they interact more effectively, as interaction energy is proportional to $S^*S/\Delta E$, where S is the overlap integral and E is the energy difference between the two orbitals. Thus, in a geometry optimization where the atoms reorganize to lower the energy of a system, a ligand with a p manifold closer to the metal d will geometry optimize to have shorter bond lengths, optimizing the interaction energy. If the manifolds are too far apart, the bond lengths will be too long for the same reason.

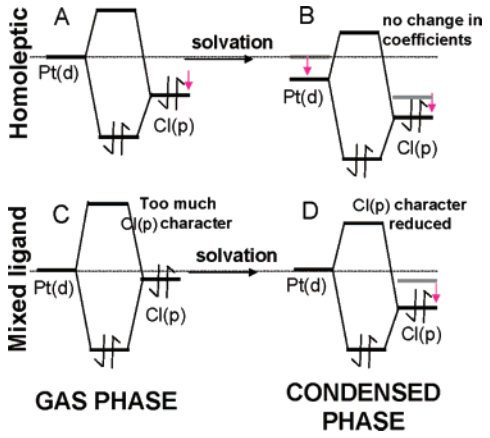

Figure 8. Simplified MO diagram for a Pt−Cl bond, showing the interaction of Pt(d) the Cl(3p) orbitals. (A) and (B) show the effect of going from gas phase to condensed phase in a system such as $[PtCl_4]^{2-}$. (C) and (D) show the effect of going from gas phase to condensed phase in a mixed-ligand system such as *cis*-$[PtCl_2(NH_3)_2]$.

In a homoleptic system, all ligands equally affect the energy of the metal d manifold. This is reflected in the difference between parts A and B of Figure 8. While both the metal d and the Cl p manifolds drop in energy when solvation is included, the energy difference between them stays approximately the same. In contrast, in a mixed-ligand system, the energy of the metal manifold has contributions from two or more different kinds of ligands. If one of them is anionic, then the addition of the solvation corrections will not affect all parts of the system in the same way, as is shown in Figure 8. In TM compounds with anionic donors and neutral donors, the anionic ligand manifold will be closer to the metal d manifold in the gas phase (Figure 7C and D). This affects the energy of a given structure because two orbitals which are closer in energy will interact more effectively (vide supra). The reverse effect (longer bond lengths) would be observed for the neutral donors in the same system.

It has been shown experimentally that the formation of cis isomers is strongly favored by polar solvents.[63] Computational studies show that this is because the cis isomer, having a dipole moment, is stabilized by a high dielectric.[62] While the stabilization of molecules with a high dipole moment is an extreme form of what is observed in this work (vide supra), it can be demonstrated that the effects of the condensed phase can be more localized than would be expected on the basis of the dipole moment of molecules alone. Figure 6 includes the orbital energy levels of both *cis*- and *trans*-$[PtCl_2(NH_3)_2]$. While they have very different dipole moments, the effects of the solvation model on the orbital energy manifolds are almost identical. Both show the Cl manifold decreasing in energy relative to the N, an effect that is absent in the homoleptic cases. If the effect were less localized (i.e., only visible in molecules with a large dipole moment), we would only see a substantial effect on the cis isomer, with the trans isomer behaving like the two homoleptic systems in the series, but this is not the case. We note that an equal effect on orbital manifolds does not imply an equal effect on bond stabilities; the stability of the cis and trans isomers of platinum complexes has a significant contribution from the symbiotic/antisymbiotic effects described by Jorgenson.[65] Two trans ligands will compete to donate electrons into the same orbital, which means that a change in orbital energies will have a larger effect on a cis isomer than on a trans isomer.

We note that the effect is different to that observed by Solomon et al., who have reported that pure density functionals are in general too covalent.[8] While the overall system may be too covalent, the effects observed here are about the *relative* interactions of different ligands.

In summary, we have examined the effects of dielectric models (COSMO and PCM) on the DFT-calculated structures of coordination compounds. It was found that gas-phase DFT calculations do not produce correct trends in the structural attributes of mixed-ligand systems which include anionic and neutral donors unless solvation corrections are included. Including solvation corrections made uniform improvements in the calculated geometric structure of coordination complexes. This effect was analyzed in terms of MO theory, and it was found that, in systems with anionic and neutral ligands, the negatively charged ligands can result in a ligand manifold with an artificially high energy relative to the rest of the system, producing an overbinding effect in the gas phase. Since the overwhelming majority of metal complex geometries are studied in condensed phases, (particularly in the crystal environment), this observation indicates that environmental effects may be important in systems where they have not been previously suspected and demonstrates the more general importance of including the effects of the environment in DFT calculations in any system where the relative strengths of ligands are important. The results further explain the correct prediction of metal−ligand bond distances by the LDA as being a consequence of LDA overbinding compensating the effects of the environment which make metal−ligand bond lengths shorter.

Acknowledgment. R.K.H. acknowledges the James Kentley Memorial, Kenneth Firth Vickery, Joan R. Clark scholarships, and the Australian government for an APA. Drs Natalie Fey, Benjamin Williams-Hubbard, and David E. Hibbs are thanked for many useful discussions during the course of this work. The Australian Centre for Advanced Computing (AC3) is thanked for access to their facilities, and the EPSRC is thanked for the Chemical Database Service. We thank the referees for their helpful suggestions on this manuscript.

Supporting Information Available: Structures of the cobalt hexaamine compounds considered herein (Figure S1), a schematic illustration of both the effect of steric bulk (Figure S2) and the effect of an anionic and neutral ligand (Figure S3), tabulation of the data given in Figure 1, (Table S1), an examination of solvation effects in organic compounds (Table S2), a statistical comparison of anionic and neutral donors for the $[NiN_nO_{6-n}]$ series (Figure S4), tabulation of the geometry-optimized crystallographic nickel bond lengths (Tables S3 and S4), tabulation of the geometry-optimized and crystallographic Pt bond lengths (Tables S5−S8), and an energy level diagram for the valence Pt orbitals (Figure S5). This material is available free of charge via the Internet at http://pubs.acs.org.

IC701166P

(65) Jorgenson, C. K. *Inorg. Chem.* **1964**, *3*, 1201−1202.